

Microscopic observation of titanomagnetite grains during palaeointensity experiments of volcanic rocks

Hidefumi Tanaka^{1,2} and Yuhji Yamamoto²

¹*Faculty of Education, Kochi University, Kochi 780-8520, Japan. E-mail: htanaka@ae.auone-net.jp*

²*Center for Advanced Marine Core Research, Kochi University, Kochi 783-8502, Japan*

Accepted 2013 September 23. Received 2013 September 23; in original form 2013 March 2

SUMMARY

Titanomagnetite (Tmt) grains, some partially maghemitized, of various oxidation levels were microscopically observed under reflected light as a function of temperature step in a Königsberger Thellier Thellier experiment in air. The reflected light microscopy indicated that the brownish colour of homogeneous Tmt turned blue at $\sim 300^\circ\text{C}$. This false blue colour was caused by submicron scale rugged stripes on the surface, according to scanning electron microscope observations, which was made after the final heating step. The typical grey-to-bluish colour of maghemitized parts of Tmt grains turned to a brownish colour at $\sim 300^\circ\text{C}$, indicating inversion of titanomaghemite to a mixture of magnetite and ilmenite (Ilm) or haematite (Hem). Although these observations were from Tmt grains on the sample surface, oxidation must have proceeded similarly within samples because the surface changes in the Tmt grains were highly correlated with behaviour of data points on Arai plots. Alterations in Tmt after heating at 610°C in air for increasing times from 10 to 500 min were evaluated by reflected light microscopy and scanning electron microscopy at the end of the experiment. Mottled patches gradually emerged in the Tmt grains during subsequent heatings. However, the formation of new Ilm lamellae was not observed, even after the final 500 min heating. In conclusion, the alteration of Tmt during laboratory heating in air at $\sim 600^\circ\text{C}$ is likely not due to the typical high-temperature oxidation that forms trellis-type Ilm lamellae. Below $\sim 400^\circ\text{C}$, the process should be closer to low-temperature oxidation. On the other hand, maghemitized parts of Tmt grains invert instantaneously at 300°C , and a trellis-type structure with Hem lamellae soon emerges when heated at 610°C .

Key words: Magnetic mineralogy and petrology; Palaeointensity; Rock and mineral magnetism.

1 INTRODUCTION

To obtain absolute palaeointensities, volcanic rocks must be heated in the laboratory, with the magnitude of the natural remanent magnetization (NRM) being compared to that of thermoremanent magnetization (TRM) given under a controlled magnetic field. Titanomagnetite (Tmt), the main remanence carrier of volcanic rocks, is notoriously prone to alteration during laboratory heat treatment. Alterations of magnetic minerals cause changes in their TRM capacity, leading to erroneous palaeointensity results. In principle, this problem can be avoided by (1) utilizing only data from heat treatments below a critical temperature at which alteration begins to proceed [Königsberger Thellier Thellier (KTT) method, Königsberger (1938) and Thellier & Thellier (1959), or (2) correcting the change of TRM capacity with that of anhysteretic remanent magnetization (ARM) [Shaw method with ARM correction, Shaw (1974), Kono

(1978) and Rolph & Shaw (1985)]. Nevertheless, the alteration of magnetic carriers in laboratory heat treatments is a major problem facing palaeointensity experiments from volcanic rocks (e.g. Valet 2003; Tauxe & Yamazaki 2007).

Changes in remanence characteristics due to sample heating are frequently studied in terms of the oxidation of Tmt. In most case studies, when samples were heated in air at $400\text{--}800^\circ\text{C}$ for several to tens of hours, drastic changes were observed in the rock magnetic characteristics, such as the saturation magnetization (M_s), Curie temperature, magnetic susceptibility (χ), TRM capacity, and others (Strangway *et al.* 1968; Larson *et al.* 1969; Creer & Petersen 1969; Davis & Evans 1976; Kono & Tanaka 1977; Kono 1985, 1987). Most researchers have interpreted the change in rock magnetic characteristics in terms of the high-temperature (deuteric) oxidation of Tmt. When high-temperature oxidation proceeds, the initially homogeneous Tmt experiences an intergrowth of titanohaematite lamellae

and Tmt host, with compositions close to ilmenite (Ilm) and magnetite (Mt), respectively (Buddington & Lindsley 1964). Hence, it is natural to correlate the change in rock magnetic properties to the result of the high-temperature oxidation in which large homogeneous Tmt grains are subdivided into smaller Mt regions. Some authors have identified an increase of Ilm lamellae in the Tmt grains of heated volcanic rock by microscopic observation (Strangway *et al.* 1968) or newly created fine Ilm lamellae by scanning electron microscope (SEM; Davis & Evans 1976). Saito (2005) performed similar laboratory heating experiments from a volcanological perspective, revealing the cooling history of a pyroclastic deposit and observing the creation and thickening of Ilm lamellae with increasing heating time.

Changes in rock magnetic characteristics observed during palaeointensity experiments are similar to those observed in laboratory heating studies. It may be that high-temperature oxidation is the cause of alteration of Tmt grains during palaeointensity experiments. However, the effects of alteration (e.g. increased TRM capacity) in palaeointensity experiments often occur at relatively low temperatures (i.e. 300–500 °C) compared to the typical temperatures (i.e. 600–800 °C) adopted in laboratory heating experiments. Additionally, the heating time for typical palaeointensity experiments (i.e. 10–15 min at plateau of temperature) differs compared to the heating time in laboratory heating investigations (i.e. a few to tens of hours). According to calculations of Yamamoto (2006), which were based on the experimental results of Mt–Tmt interdiffusion reported by Freer & Hauptman (1978), it should take months to create even a fine Ilm lamellae of 0.01 µm thick at ~350 °C. Hence, it is not obvious that the high-temperature oxidation of Tmt grains is responsible for alterations in magnetic minerals in palaeointensity experiments.

Low-temperature oxidation (also called maghemitization) is a single-phase oxidation process that usually occurs below 200–300 °C. As low-temperature oxidation proceeds, the spinel structure of Tmt is maintained, resulting in cation-deficient Tmt (called titanomaghemite, Tmh). Low-temperature oxidation occurs under various natural conditions, including oceanic basalt (e.g. Ozima 1971; Johnson & Atwater 1977), marine sediment (e.g. Kent & Lowrie 1974), loess (e.g. Liu *et al.* 1992, Chen *et al.* 2005) and subaerial rocks (e.g. Akimoto & Kushiro 1960, Ozima & Larson 1967, Allan *et al.* 1989). As these cases are, to some extent, related to hydrothermal alteration or prolonged weathering in which water is circulated, water is generally considered to be necessary for low-temperature oxidation. Hence, it is difficult to suppose that low-temperature oxidation occurs during heating in palaeointensity experiments. However, Creer *et al.* (1970) reported a case in which low-temperature oxidation was suspected during laboratory heatings of basalt at 400 °C in air for increasing times from 10 min to 88 hr.

Alteration of Tmt grains during laboratory heating is not always caused by high- or low-temperature oxidation. Subaerial volcanic rocks sometimes suffer from low-temperature oxidation of Tmt grains due to weathering. When these rocks samples, which include maghemitized Tmt grains, are heated in the laboratory up to 300–400 °C, Tmh easily inverts to a mixture of Mt and Ilm or haematite (Hem) (O'Reilly 1983). As Tmh inversion occurs regardless of furnace atmosphere, air or vacuum (Ozima & Larson 1970), this event can lead to a severe problem in palaeointensity experiments.

Observations of magnetic minerals through optical and electron microscopy or by recently developed sophisticated techniques, such as magnetic force microscopy, have contributed tremendously to the field of rock magnetism and magnetic mineralogy (e.g. Haggerty

1991; Dunlop 2012). An electron probe microanalysis by Furuta *et al.* (1985) established the oxidation process of iron removal in the low-temperature oxidation of submarine basalt, which had been suggested by other rock magnetic studies (e.g. Marshall & Cox 1972; Ryall & Hall 1980). Watkins & Haggerty (1967) demonstrated a clear correlation between the magnitude and stability of lava remanence and the level of high-temperature oxidation of Tmt, which was classified by Wilson & Watkins (1967). A study by Davis & Evans (1976) incorporating electron microscope observations revealed the importance of high-temperature oxidized Tmt grains with lamellae intergrowth to remanence stability.

In spite of the potential of microscopic observations to address various problems in palaeointensity experiments, only a few studies have used this approach (e.g. Yamamoto *et al.* 2003; Yamamoto & Hoshi 2008). The aim of the study described in this paper was to clarify the mechanism of alteration of magnetic carriers, through observing Tmt grains by optical microscopy at each step of KTT experiments. No previous study of magnetic minerals at every step has been performed, except for Holm & Verosub (1988), in which magnetic carriers of marine sediments were observed by SEM during thermal demagnetization.

We also performed microscopic observations in typical laboratory heating experiments on a sample heated at 610 °C in air for increasing times from 10 to 500 min. We employed a series of experiments with the same heating temperatures and times as used by Tanaka & Komuro (2009), in which validity and limitations of ARM correction in the Shaw experiments were studied, to obtain its magneto-mineralogical background.

Microscopic observations were made on large multidomain (MD) grains, which might not be related to the behaviour of the remanence that should be predominantly carried by single-domain (SD) and/or pseudo-single-domain (PSD) grains. Nevertheless, we think that the alteration that occurs in MD grains will also proceed in smaller SD/PSD grains with even higher rates.

2 SAMPLES

Four volcanic rock samples were used in this study: (1) Cretaceous basalt from Inner Mongolia, northeastern China (CP0106B), (2) 1983 AD basalt lava from the Miyakejima Volcano, Japan (MY070132), and (3) glassy part of 500 Ka (OT572261) and (4) massive part of 740 Ka (OT580411) andesite lavas from the Ontake Volcano, Japan. CP0106B is a pristine sister sample of one of the lava samples used by Tanaka & Kono (2002). The other three samples are pristine sister samples of those used by Tanaka & Komuro (2009). CP0106B and MY070132 were used during the KTT experiment. OT572261 and OT580411 were used in the heating experiment at 610 °C for progressively longer heating times.

Samples were prepared as a plate of ~10 mm in thickness and 25 mm in diameter. The top surface was polished with diamond paste of 1 µm in grain size for observations under reflected light microscopy or SEM. Optical and electron microscopic observations were performed with Metaphoto (Nikon Corporation, Tokyo, Japan) and JSM-6500F (JEOL Ltd., Tokyo, Japan) equipment, respectively. The chemical composition of Tmt grains was occasionally measured in the SEM observation by energy dispersive spectroscopy (EDS).

Before the palaeointensity experiments were performed, pristine samples were examined by optical microscopy and SEM, to obtain a general view of compositions and oxidation levels of magnetic minerals. Oxidation levels of Tmt grains were determined based on surface texture under optical microscope following Haggerty

Table 1. Magnetic carriers of the volcanic rock samples.

Sample	Rock type	Magnetic mineral	Composition	Grain size (μm)	Oxidation level
CP0106B	Basalt	Tmt (partially maghemitized)	~ 0.7	5–100	C1 (partially low-T oxidized)
MY070132	Basalt	Tmt	0.05–0.4	1–20	C1–C5
OT572261	Andesite	Tmt	0.1–0.4	0.5–20	C1
OT580411	Andesite	Tmt (partially maghemitized)	0.2–0.4	5–100	C1–C3 (partially low-T oxidized)

Note: Composition, Usp content (x) of Tmt; oxidation level, classification by Haggerty (1991).

(1991): homogeneous ulvospinel (Usp)-rich Tmt (C1), Mt-enriched Tmt with a small number of Ilm lamellae (C2), Ti-poor Tmt with densely crowded Ilm lamellae (C3), additional oxidation with indistinct mottling of Ilm lamellae and the development of metaimenite (C4), further oxidation characterized by the development of rutile and titanohaematite within the metaimenite (C5), incipient formation of pseudo-brookite from the rutile and titanohaematite (C6), and the most advanced level characterized by the assemblage of pseudo-brookite and Hem (C7).

Magnetic minerals of CP0106B were homogeneous Tmt with $x \sim 0.7$, where x is a mole fraction of Usp. Typical grain sizes of these minerals ranged from 1 to 50 μm . About 50 per cent were maghemitized to Tmh along the grain periphery and cracks. This maghemitization was not reported in Tanaka & Kono (2002) because microscopic observation was not performed in the original study. Magnetic minerals of MY070132 were fine Tmt grains (1–5 μm) that existed in various oxidation levels, from homogeneous (C1) to highly oxidized (C4 or C5). They occasionally include grains of ~ 50 μm or larger. Magnetic minerals of OT572261 were very fine (~ 1 μm or smaller) homogeneous Tmt, with x ranging from 0.1 to 0.4. Occasionally, large homogeneous grains of 10–50 μm were included. Magnetic minerals of OT580411 were originally Tmt grains with various oxidation levels (C1–C3). Roughly half of them were maghemitized to Tmh along the periphery and cracks, although, similar to CP0106B, this maghemitization was not described in Tanaka & Komuro (2009). Characteristics of the magnetic minerals are described in Table 1.

3 EXPERIMENTS AND MICROSCOPIC OBSERVATIONS

3.1 Alterations during KTT experiment

The KTT experiment, using the protocol by Coe (1967a), was performed on basalt samples CP0106B and MY070132 in air. About 20 Tmt grains from each sample were selected for optical microscopic observation after each step of the experiment. Photographs were taken under reflected light with magnifications of $\times 600$ and $\times 1000$. SEM image with various magnifications were taken after completion of the KTT experiment.

The experiment was concluded at 400 $^{\circ}\text{C}$ for CP0106B because of its low blocking temperature. Throughout the experiment, grain surface alterations differed between homogeneous and partially maghemitized grains. Fig. 1 shows representative photographs of selected steps for a homogeneous Tmt grain (a), Tmt grain with Tmh at the periphery (b) and an Arai plot (Nagata *et al.* 1963) of the KTT experiment (c). Scale bars in the photographs indicate 10 μm . In each series, the final photograph shows the grain subsurface at the end of the experiment after scraping the top altered

surface. The subsurface layer was considered to be a few microns below the original surface.

The typical brown-to-tan colour of the homogeneous Tmt grain turned bluish at 250 $^{\circ}\text{C}$ and became dark blue above 300 $^{\circ}\text{C}$ (Fig. 1a). This peculiar blue colour invaded only the surface, reaching a depth of a few microns at most. This is because after the last heating step and repolishing, the subsurface showed the typical brownish colour of Tmt, although it was more reddish than usual, possibly due to oxidation.

The Tmh part of partially maghemitized Tmt grain showed a much different colour change (Fig. 1b). The typical grey-to-bluish colour of Tmh turned brownish at 300 $^{\circ}\text{C}$, but the unoxidized part showed a similar colour change as the homogeneous Tmt grain in Fig. 1(a). The grey-to-bluish colour of the Tmh part was intrinsic to the mineral. The change to brownish colour at 300 $^{\circ}\text{C}$ indicated inversion of Tmh to a mixture of Tmt with low Usp content and Ilm or Hem, although no lamellae structure was observed.

The Arai plot revealed a linear relation between NRM lost and TRM gained, which is shown in a solid line in Fig. 1(c). The data points exhibited scatter starting at 250 $^{\circ}\text{C}$, coinciding with the temperature of the first appearance of the bluish colour in Figs 1(a) and (b).

The second sample MY070132 was observed with wider temperature steps, up to a higher maximum of 560 $^{\circ}\text{C}$. The surface colour of Tmt grains turned blue around 300–400 $^{\circ}\text{C}$, similar to the first sample CP0106B (Fig. 1). However, the surface alterations were more severe in the later experimental stages, due to the much higher temperatures of the final steps. Tmt grains of MY070132 were free of maghemitization, but the level of high-temperature oxidation differed among different grains (oxidation levels of C1–C5). Fig. 2 shows series of photographs for three representative Tmt grains with oxidation levels C1 (a), C3 (b) and C5 (c), together with an Arai plot of the KTT experiment (d). The last photograph of the series shows the appearance of the subsurface, a few microns below the original surface, after the final heating step.

When we compared the three series of photographs in Figs 2(a)–(c), we observed that alterations of the Tmt grains during the experiment were more severe for those of lower oxidation level. For example, whereas the Tmt grain of C1 oxidation level (Fig. 2a) demonstrated a complicated false colour outcome at 560 $^{\circ}\text{C}$, the C5 grain (Fig. 2c) showed little change in appearance. For each grain, the subsurface showed no sign of alteration, as shown in the last photographs of the series, except for a more reddish colour that was possibly due to oxidation.

The Arai plot of this sample (Fig. 2d) revealed that TRM gain increased at ≥ 440 $^{\circ}\text{C}$, coinciding with the temperature range of severe changes in the surface appearance of Tmt grains in Figs 2(a) and (b). The temperature of initiation of bluish colour at ~ 300 $^{\circ}\text{C}$ did not seem to be related to scatter in the Arai plot. Nevertheless, the test of partial TRM (pTRM) at 300 $^{\circ}\text{C}$ was negative when the

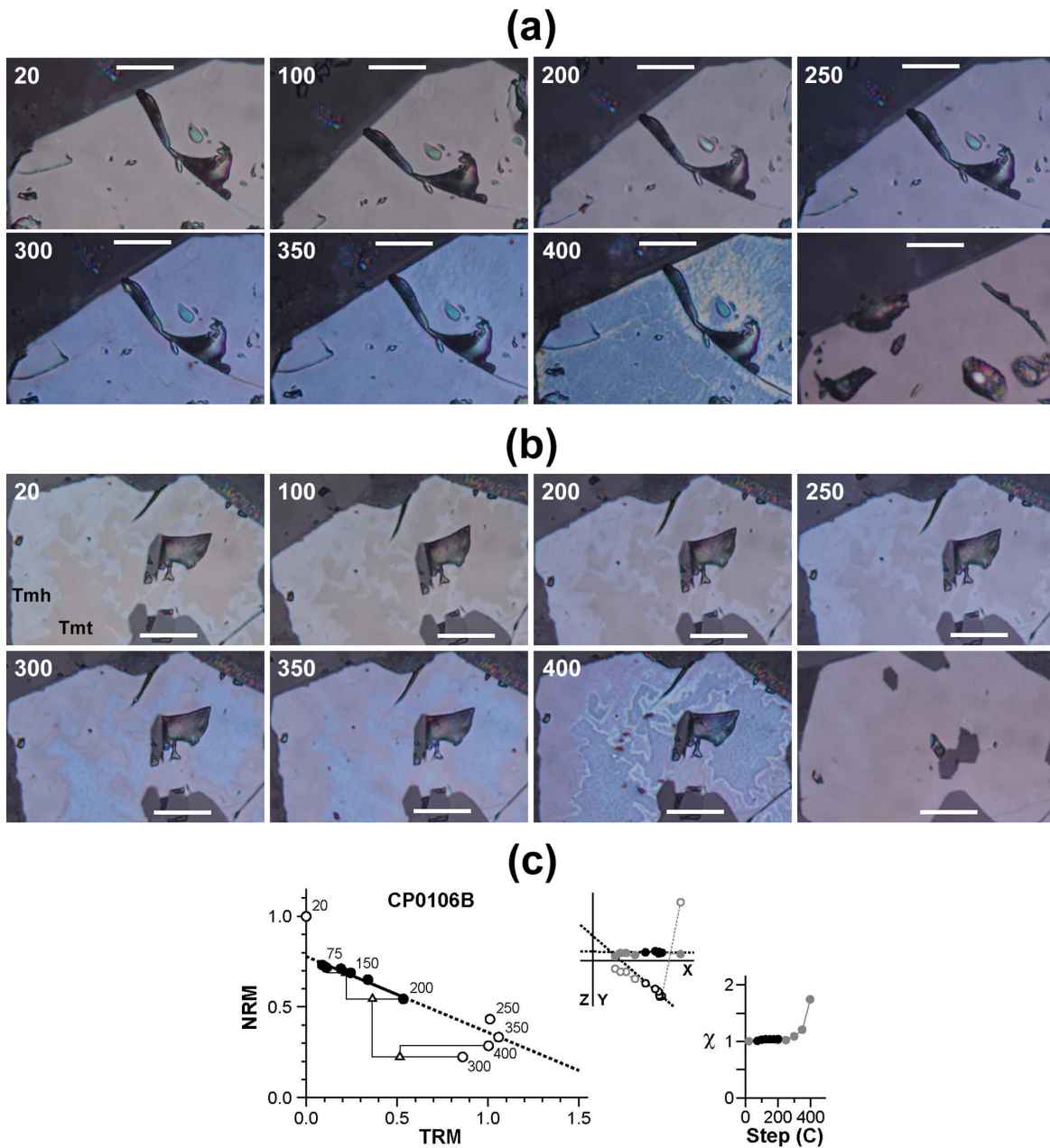


Figure 1. Change of colour and morphology of two representative Tmt grains on the surface of a basalt sample CP0106B during a KTT experiment. Each photograph is a half-crop from the original image of 4256×2832 pixels, which was taken with $\times 1000$ magnification ($\times 10$ eyepiece with $\times 100$ object lens) under reflected light. Series of photographs are for homogeneous (a) and half maghemitized (b) titanomagnetite, where a white bar indicates a scale of $10 \mu\text{m}$ and the number is the temperature of selected step. The last photograph of each series shows the subsurface of the grain at the end of the experiment, which was prepared by scraping the altered surface with $1 \mu\text{m}$ diamond paste after the last heating step at 400°C and after subsequent SEM observation. In the first photograph of half maghemitized titanomagnetite (b), maghemitized and unoxidized host parts are indicated by black letters of Tmh and Tmt, respectively. Results of the KTT experiment (c) are shown on an Arai plot together with an orthogonal plot of NRM direction at zero field steps and a curve of magnetic susceptibility versus temperature step. On the Arai plot, a thick line shows the best fitted linear relation of NRM and TRM and triangles are the data points of pTRM checks. Solid and open circles on the orthogonal plot indicate projections on horizontal and vertical planes, respectively. Results of Arai plot analysis are summarized in Table 2.

conventional criterion of 7 per cent for the difference ratio (DRAT) was applied.

After the KTT experiment was completed at the 400°C and 560°C steps for CP0106B and MY070132, respectively, SEM images of the altered surfaces and subsurfaces of the Tmt grains were obtained. For the homogeneous Tmt grain of CP0106B, Figs 3(a) and (b) show the original optical microscopic photograph and the backscattered electron (BSE) image, respectively, of the blue-

coloured surface at 400°C step. The high-magnification ($\times 50\,000$) secondary electron image (SEI) and BSE image for the rectangular area in Fig. 3(b) are shown in Figs 3(c) and (d), respectively, which showed rugged surface. This is contrasted to a smooth surface of Tmt grains of a pristine sample shown in the bottom row of Figs 3(m)–(p). Fig. 3(m) is an optical microscopic photograph of a sister sample, with Fig. 3(n) showing a high magnification BSE image for the yellow rectangular area. The smooth surface in

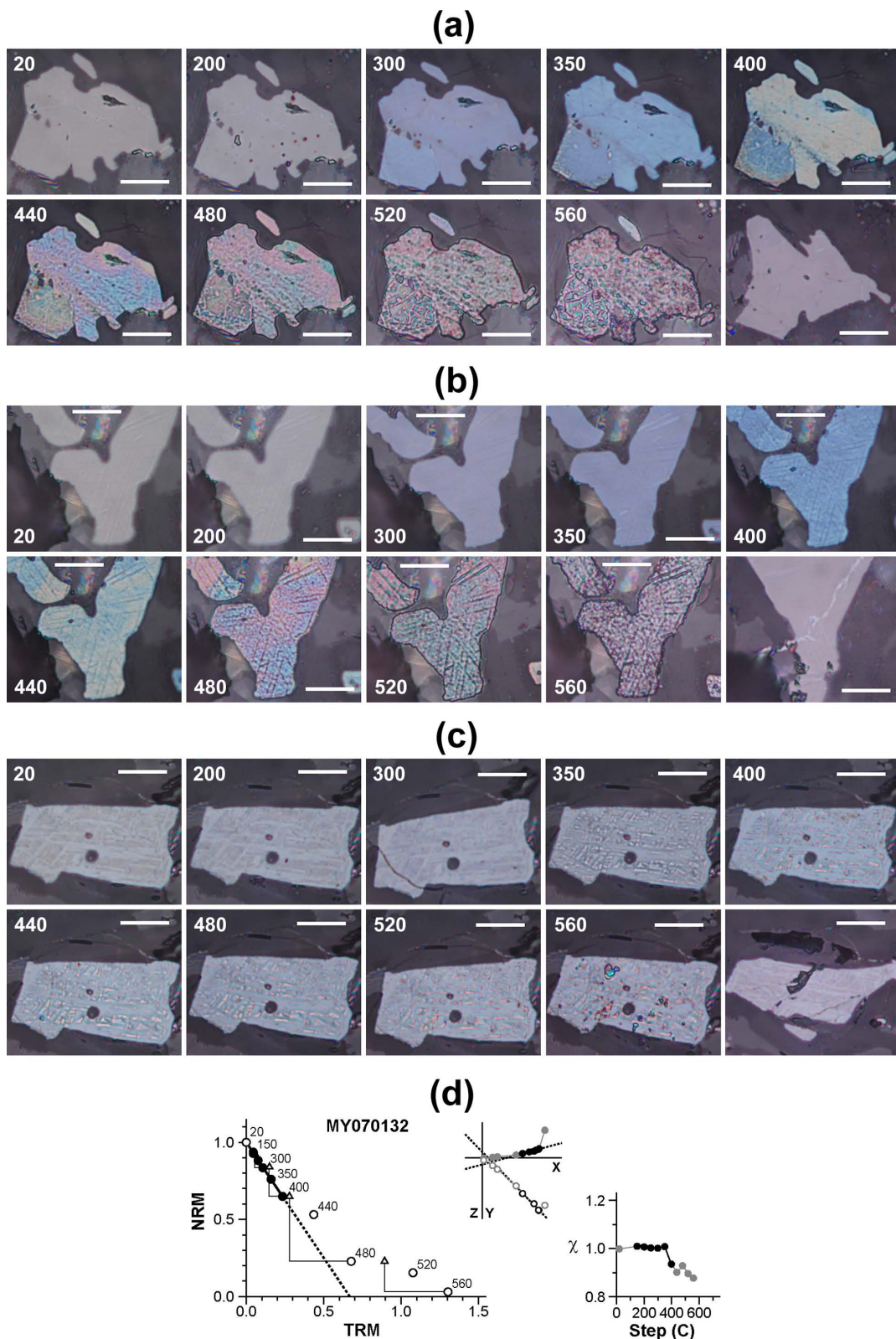


Figure 2. Change of colour and morphology of three representative Tmt grains on the surface of a basalt sample MY070132 with higher blocking temperatures than the sample shown in Fig. 1. The oxidation level following Haggerty (1991) of the Tmt grains at the initial pristine state are C1 (a), C3 (b) and C5 (c). A white bar indicates a scale of 10 μm throughout the images. Results of the KTT experiment are shown in (d). For the details of symbols and numbers, see the caption of Fig. 1.

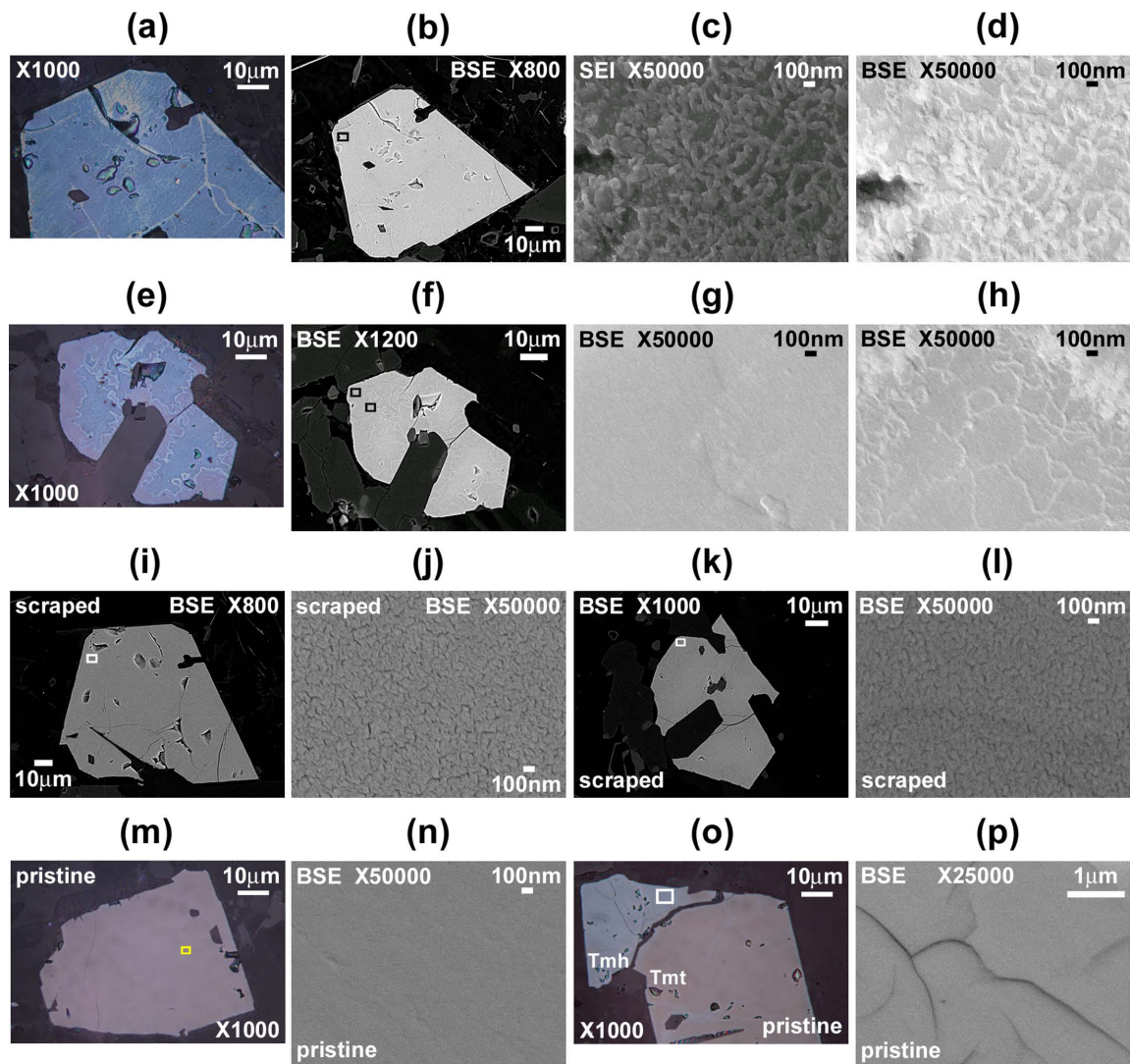


Figure 3. Altered surface of Tmt after the last step of 400 °C for the homogeneous (a–d) and partly maghemitized (e–h) grains of CP0106B. Original optical microscopic photographs of Figs 1(a) and (b) are shown in (a) and (e), respectively, and their BSE images are shown in (b) and (f), respectively. The high-magnification ($\times 50000$) SEI and BSE image for the rectangular area in (b) are shown in (c) and (d), respectively. BSE images of two rectangular areas at upper left-hand side of (f) are shown in (g) and (h); (g) was originally maghemitized but now appears brownish, and (h) was originally homogeneous but now appears dark blue. Low- and high-magnification BSE images of subsurface after scraping the altered surface are shown in (i) and (j) for the homogeneous grain and in (k) and (l) for the partly maghemitized grain. Microscopic photographs and high-magnification BSE images of Tmt grains in a pristine sister sample are shown in the bottom row (m–p). (m) and (n) are homogeneous Tmt grain and (o) and (p) are partly maghemitized grain. In the latter, maghemitized and unoxidized parts are indicated in white letters of Tmh and Tmt, respectively (o) and the high-magnification BSE image (p) shows maghemitized part.

Figs 3(m) and (n) was clearly different from the rugged surface of the altered grains in Figs 3(c) and (d), allowing us to conclude that the rugged, striped surface was the cause of the false blue colour.

The original photograph of the partially maghemitized grain of CP0106B at the 400 °C step and its BSE image are shown in Figs 3(e) and (f), respectively. Fig. 3(g) is the high-magnification BSE image of the rectangular area at the upper left-hand side corner in Fig. 3(f), which was originally maghemitized, but now appears brownish. Fig. 3(h) is the high-magnification BSE image of the rectangular area at the lower right-hand side from the former in Fig. 3(f), which was originally homogeneous Tmt host but now appears dark blue. The surface of the former was smooth, whereas the latter was rugged with stripes.

BSE images of the subsurfaces of the same grains (after re-polishing) are shown in the third row of Fig. 3. Figs 3(i) and (j)

are images of the subsurface of the homogeneous grain shown in (a)–(d). Figs 3(k) and (l) are images of the subsurface for the maghemitized grain shown in (e)–(h). The white rectangular areas in low magnification images (i) and (k) were enlarged by $\times 50000$ and are shown in (j) and (l), respectively. On reflected light microscopy, the surfaces of these areas were a normal brownish colour, although more reddish than the originals shown in the last photographs of Figs 1(a) and (b). Nevertheless the enlarged BSE images of Figs 3(j) and (l) showed a complicated appearance, with many whisker-like microfractures. As mentioned earlier, Tmt grains in the pristine sister sample lacked these microfractures (Figs 3m and n). The maghemitized part of Tmt grains in the pristine sample (Figs 3o and p) also lacked these microfractures. In the high-magnification image of the maghemitized part (Fig. 3p), the surface was smooth, although the shrinkage cracks typical for Tmh can be clearly seen (Petersen & Hojatollah 1987).

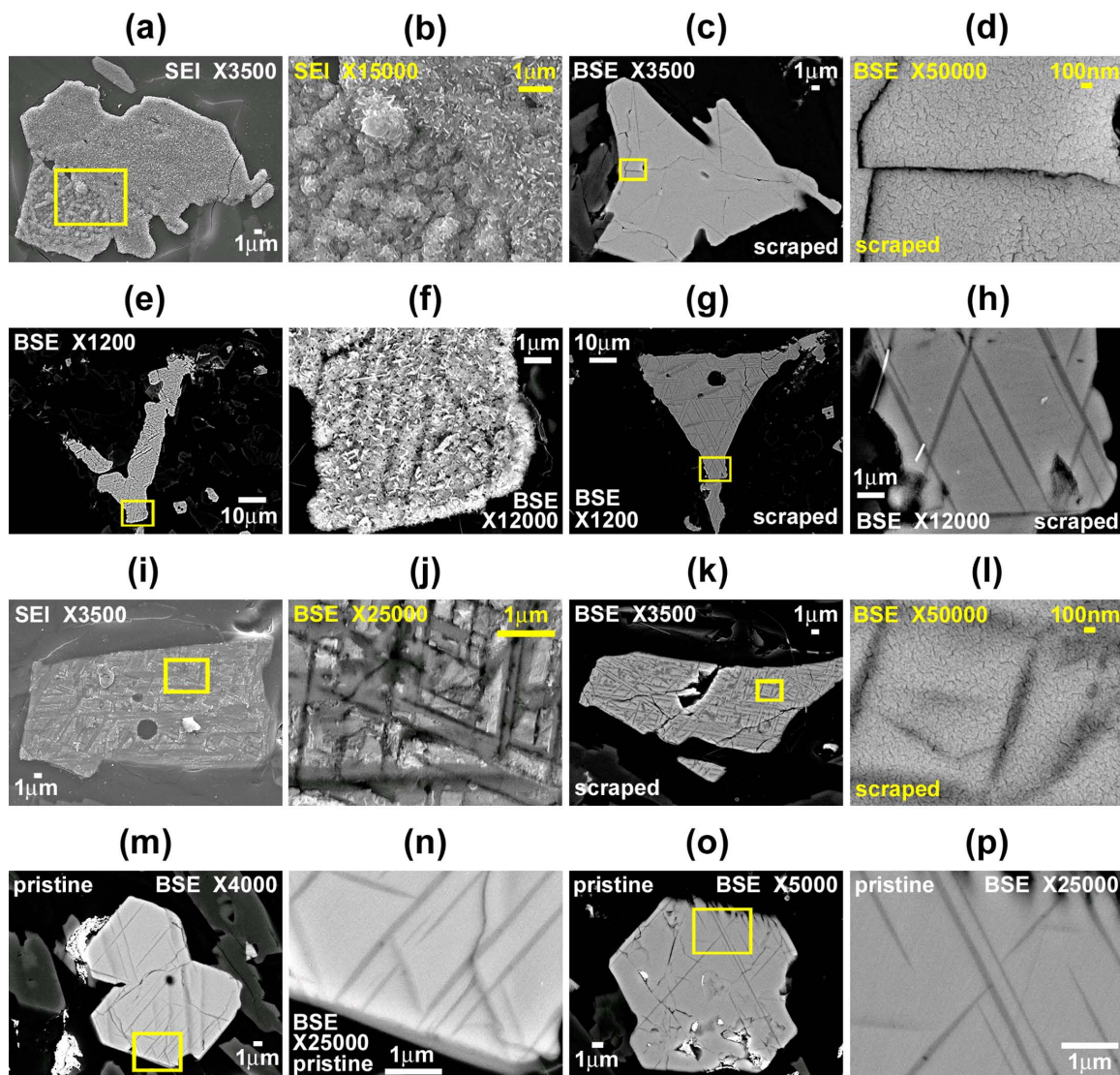


Figure 4. Top three rows show SEM images of three Tmt grains of MY070132 after the final step of 560 °C. Original oxidation levels of the Tmt grains were C1 (a–d), C3 (e–h) and C5 (i–l). Photographs in the two left-hand columns show altered top surface (a, b, e, f, i, j) and scraped subsurface are shown in the two right-hand columns (c, d, g, h, k, l). Rectangular area in the low-magnification images were enlarged and are shown beside each of the low-magnification images. Bottom row (m–p) shows Tmt grains of C3 oxidation level in a pristine sister sample.

SEM images of Tmt grains of MY070132 at the 560 °C step and those of the subsurface are shown in the top three rows of Fig. 4. Oxidation levels of the Tmt grains in the initial pristine state were C1 (a–d), C3 (e–h) and C5 (i–l). Yellow rectangular areas in the low-magnification images were enlarged and are shown beside each of the low-magnification images. Images of the altered surfaces of the Tmt grains shown in the two left-hand columns of Figs 4(a), (b), (e), (f), (i) and (j) revealed that the surface roughness was less severe for grains of higher oxidation level. SEM images of the subsurfaces shown in the two right-hand columns of Figs 4(c), (d), (g), (h), (k) and (l) did not indicate any major structural changes of Tmt, such as the creation of new Ilm lamellae, at least for the low- to medium-magnification images (Figs 4c, g, h and k). Nevertheless, the peculiar appearance of many microfractures in the high-magnification images (Figs 4d and l) indicated that the alteration had penetrated to a depth of more than several microns. These microfractures were products of alteration because there was no such feature in the Tmt grains of the pristine sister sample. BSE images in the bottom row of Figs 4(m)–(p) were taken from two Tmt grains of C3 oxidation

level in a pristine sister sample. A smooth surface was seen in the high-magnification images (Figs 4n and p) of each grain.

3.2 Alteration during progressively longer heatings at 610 °C

In a second series of experiments, we observed alterations of the Tmt grains by optical microscope under reflected light while heating two andesite samples (OT572261 and OT580411) at 610 °C in air for increasing times of 10, 20, 50, 100, 200 and 500 min. About 20 Tmt grains were observed in each sample. Because the first experiment revealed that the false colour of the altered Tmt grains was caused by the top thin rugged surface, microscopic observations were made on the subsurface, prepared by scraping the surface with a 1 μm diamond paste after each run of heating experiments. In the following, one representative result from each sample is given. After the final heating run of 500 min, SEM observation was made. As the initial pristine state of the Tmt grains of these two samples

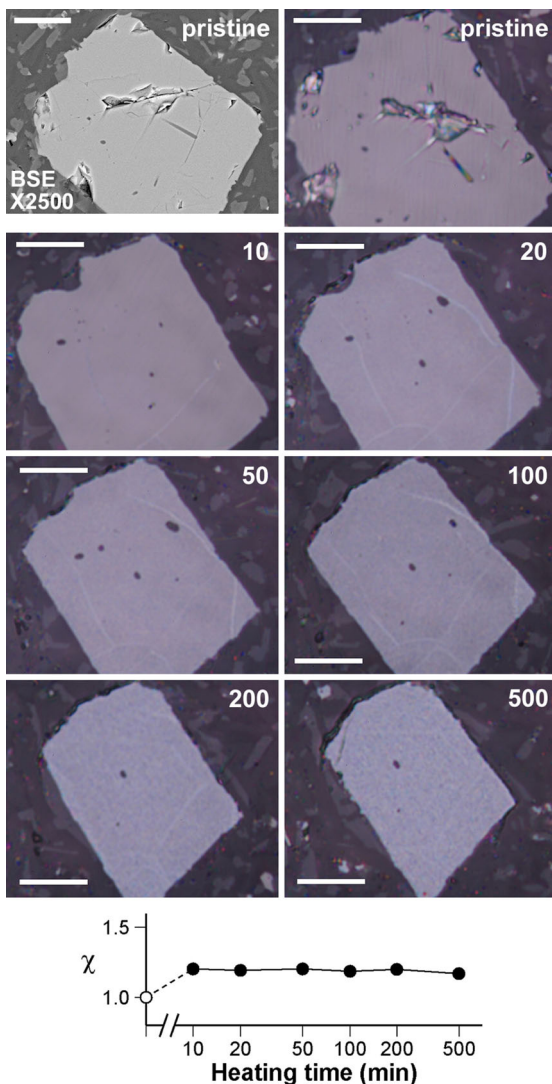


Figure 5. Change of morphology of a homogeneous Tmt grain of andesite sample OT572261 during heating at 610 °C in air for increasing times. The first two photographs are BSE and optical images in the initial pristine state and series of optical images follow, where the number is the heating time in minutes and scale bars indicate 10 μm . Note that the grain size gradually decreased as the experiment proceeded because the top surface was scraped after each heating run. Bottom graph shows change of magnetic susceptibility versus heating time, where the abscissa is in log scaling.

had been observed by SEM, we were able to clarify changes in the Tmt grains on the basis of SEM images.

Fig. 5 shows the results from a Tmt grain of OT572261 with an oxidation level of C1. The first two photographs are BSE and optical images of the initial pristine state, which are followed by a series of optical microscopic photographs. The scale bar is 10 μm , and the number is the heating time in minutes. The change in the magnetic susceptibility versus heating time is also shown at the bottom of the figure. The grain size gradually decreased as the experiment proceeded because the top surface was scraped after each heating run. The change in surface appearance was not drastic, but a slight loss of brown colour was recognized after a 20-min heating run. Small bluish patches appeared after a 50-min heating run, which spread all over the grain after the final 500-min heating run. Magnetic susceptibility increased by 20 per cent after the first heating of 10 min and was constant thereafter.

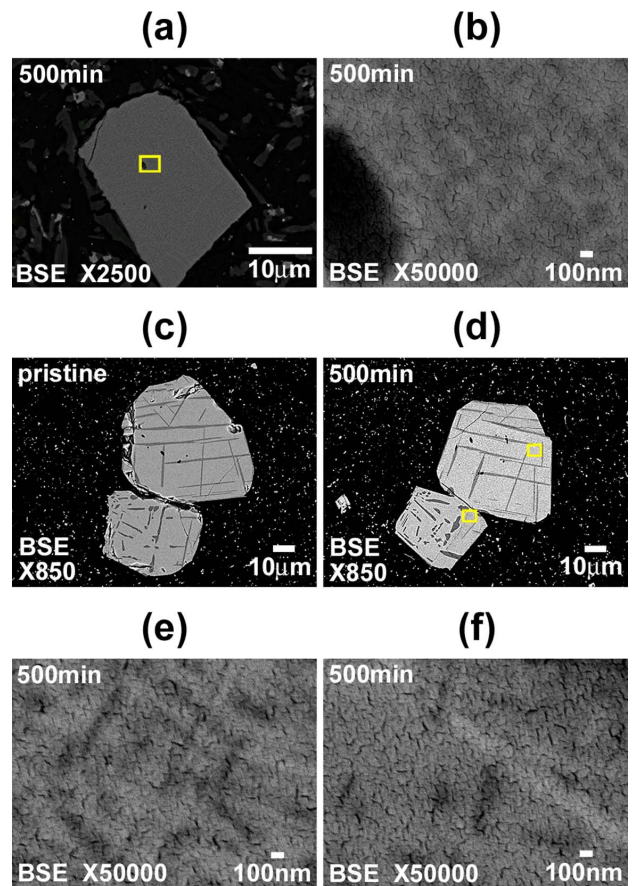


Figure 6. BSE images of two Tmt grains of OT572261 after the final heating run of 500 min: (a) and (b) show low and high magnification images, respectively, of the grain shown in Fig. 5. BSE images of another grain of C2 oxidation level are shown in pristine state (c) and after final run (d). High-magnification BSE images of the yellow rectangular areas at the lower left-hand side and upper right-hand side in (d) are shown in (e) and (f), respectively.

Fig. 6(a) shows a BSE image of this grain after the final heating run. The yellow rectangular area was enlarged by $\times 50\,000$ (Fig. 6b), revealing that the dark patches on the BSE image were the cause of the mottled appearance on the optical microscopic photographs. Many small whisker-like microfractures appeared, as was the case in the KTT experiment.

Figs 6(c)–(f) show the BSE images of another Tmt grain of C2 oxidation level. Low-magnification BSE images indicated that the Tmt host part of the grain was mottled after the final heating run (Fig. 6d), whereas the pristine state was smooth (Fig. 6c). There was no difference in Ilm lamellae between the pristine state (Fig. 6c) and the altered grain (Fig. 6d). However one-to-one correspondence of lamellae is difficult because the surface observed after the final heating run was deeper than the original layer by more than $\sim 10\ \mu\text{m}$, due to the multiple polishing. High-magnification BSE images of the yellow rectangular areas at the lower left-hand side and upper right-hand side in Fig. 6(d) are shown in Figs 6(e) and (f), respectively. There was some regularity in the distribution of the dark patches, especially in the image of Fig. 6(e).

Fig. 7 shows a representative result from another andesite sample (OT580411), in which about half of the Tmt grains were maghemitized. The Tmt grain shown in Fig. 7 was completely maghemitized. This grain was originally at an oxidation level of C2, judging from the presence of a thick Ilm lamellae and sporadic fine lamellae.

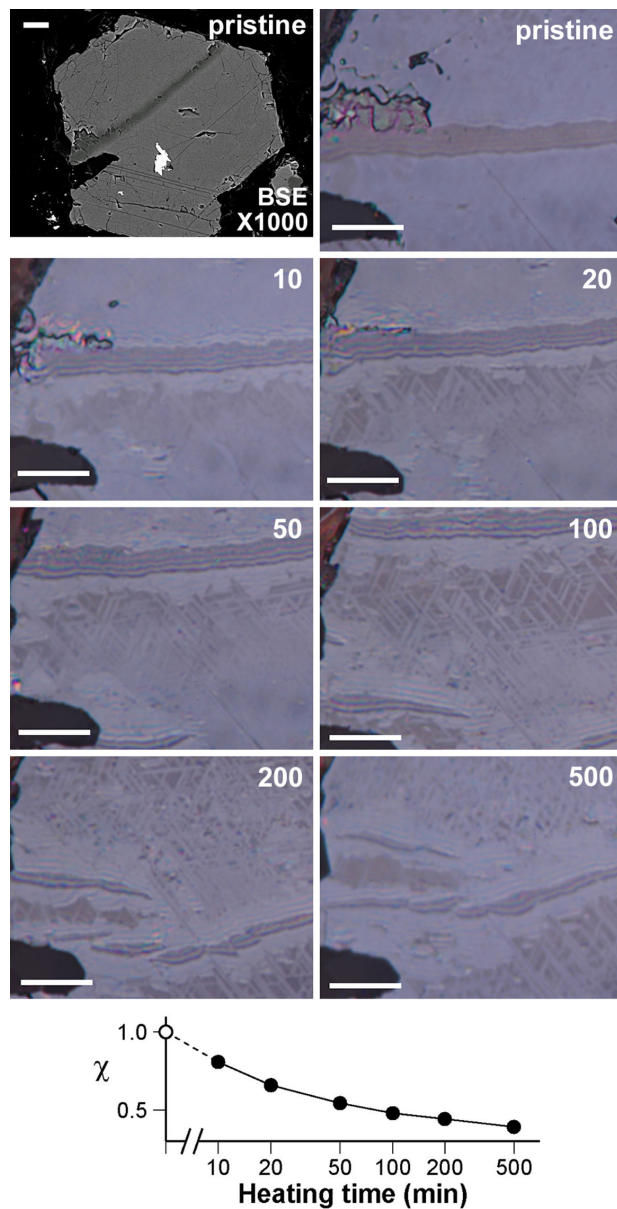


Figure 7. Change of morphology of a completely maghemitized Tmt grain of andesite sample OT580411 during heating at 610 °C in air for increasing times. A trellis-type structure developed as the heating experiment proceeded. The magnetic susceptibility decreased drastically with heating time (bottom graph). For the details of symbols and numbers, see the caption of Fig. 5.

Fig. 7 clearly shows that a trellis-type structure developed as the heating experiment proceeded. This structure appeared only after the first 10 min heating run. The magnetic susceptibility decreased drastically with heating time (bottom graph of Fig. 7). After the final 500 min heating run, χ was 39 per cent of the initial value of the pristine state.

SEM images of this grain are shown in Figs 8(a)–(d). Fig. 8(a) shows a BSE image of the pristine state at $\times 3000$ magnification, covering the lower left-hand side part of the first image of Fig. 7. Many cracks typical of Tmh were clearly seen. Nearly the same area of the grain that was altered after the final 500 min heating run is shown in the BSE image of Fig. 8(b) under the same magnification. The altered grain surface showed a well-developed trellis-type structure. Fig. 8(c) shows another BSE image of the same grain after

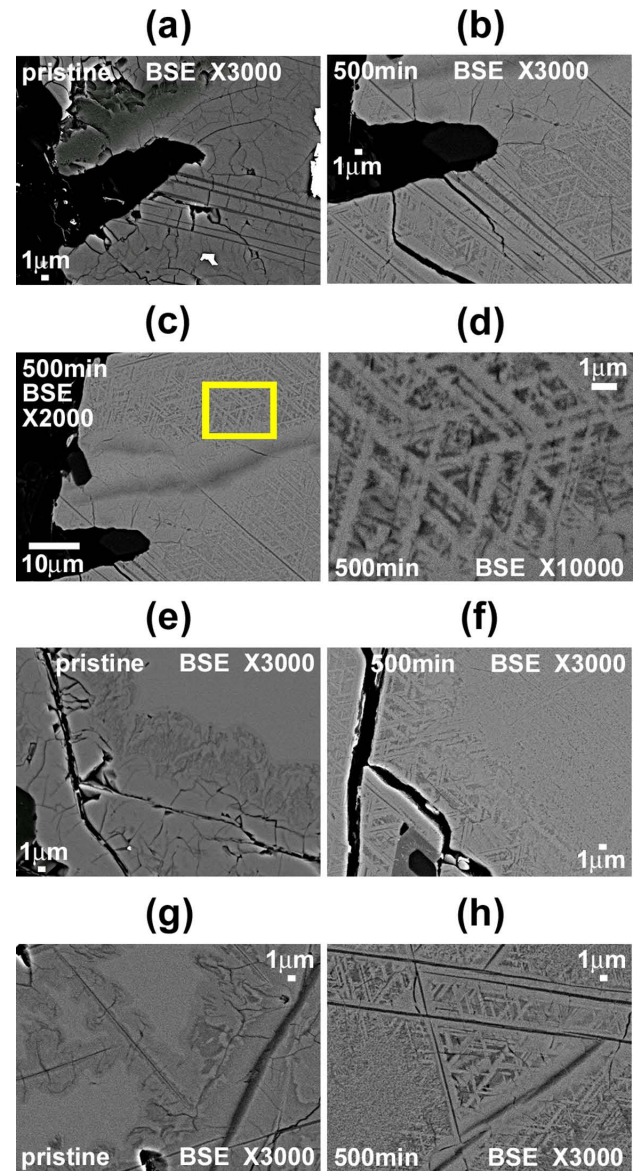


Figure 8. BSE images of the completely maghemitized Tmt grain shown in Fig. 7 in pristine state (a) and after the final 500 min heating run (b–d). Rectangular area in (c) is shown in (d) with enlarged magnification. BSE images of two other partially maghemitized Tmt grains are shown in (e–h). Initial pristine state is shown in the images on the left-hand side (e, g). The images on the right-hand side are of the altered surface of the same grain (f, h) after the final 500 min heating run.

the final heating run, with Fig. 8(d) showing an image with $\times 10\,000$ magnification of the yellow rectangular area. The trellis-type structure was obviously along the $\{111\}$ plane of the spinel structure. As will be discussed later, we think that these trellises are lamellae of Hem produced by inversion of Tmh, although it was difficult to identify their chemical composition due to their fine scale compared to the size of the electron microscope beam.

SEM images of two other representative grains are shown in the third and bottom rows of Fig. 8. Homogeneous Tmt host remained at the centre in the initial pristine state shown in the images on the left-hand side (Figs 8e and g). The images on the right-hand side are of the altered surface of the same grain, more than 10 μm below from the original surface, after the final 500 min heating run (Figs 8f and h). In the latter images, the boundary between the central unoxidized

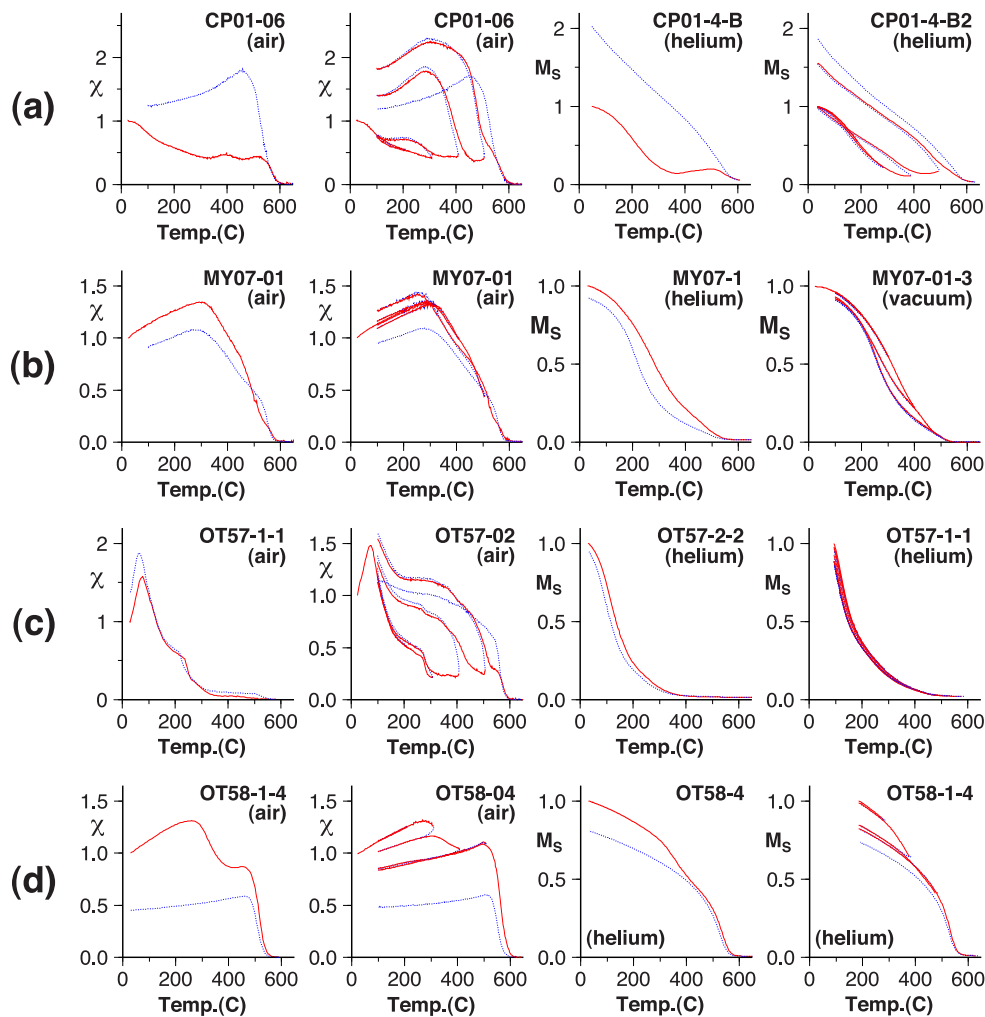


Figure 9. $\chi - T$ and $M_S - T$ curves for sister samples of the four samples used in this study. Red solid and blue dotted lines indicate heating and cooling runs, respectively. Second from the left and rightmost graphs show $\chi - T$ and $M_S - T$ curves, respectively, to progressively elevated temperatures. Progressive $\chi - T$ curve of OT57-02 [second graph from the left-hand side in panel (c)] is incompatible with other measurements of the same lava flow. The specific sample was seemingly suffered from maghemitization, possibly due to weathering.

part and the surrounding maghemitized part became smeared, and the trellis-type structure was well developed along the originally maghemitized part.

3.3 Temperature dependence of magnetic susceptibility and saturation magnetization

Supplemental measurements were made to obtain $\chi - T$ and $M_S - T$ curves using sister samples of the four samples experimented in this study. $\chi - T$ curves were measured in air with either a magnetic susceptibility system (MS2) from Bartington Instruments Ltd. (Witney, England, U.K.) or a Kappabridge (KLY-3S) of Agico Inc. (Brno, Czech Republic). $M_S - T$ curves were measured in helium with a vibrating sample magnetometer (VSM; Micromag 3900) from Princeton Measurements Co. (Westerville, Ohio, U.S.A.) except for MY07-01-3, which was measured in vacuum with a magnetic balance (NMB-89) of Natuhara-Giken (Osaka, Japan).

Results are summarized in Fig. 9 in which left- and right-hand two columns show $\chi - T$ and $M_S - T$ curves, respectively. Progressive $\chi - T$ and $M_S - T$ curves with 100 °C increment are shown in the second graph from the left and the rightmost graph, respec-

tively. Magnetic hysteresis parameters were also measured for sister samples with the VSM. They are summarized on a Day plot (Day *et al.* 1977) shown in the Appendix.

$\chi - T$ and $M_S - T$ curves of CP01 show a drastic increase in the cooling run (Fig. 9a), which is often seen in oceanic basalt, indicating presence of Tmh. Progressive curves indicate that the inversion of Tmh occurred at 300–400 °C, which is in agreement with the microscopic observation during the KTT experiment. $\chi - T$ and $M_S - T$ curves of OT58 showed a decrease of χ and M_S at 300–400 °C (Fig. 9d), which is also an indication of Tmh inversion. Slight decrease of χ and M_S in the cooling run was observed for MY07 (Fig. 9b) and the progressive curves indicated 400–500 °C for its occurrence. $\chi - T$ and $M_S - T$ curves of OT57 showed almost no change between heating and cooling runs (Fig. 9c). An exception is the progressive χ measurements in air of OT57-02 (second graph from the left-hand side), which is incompatible with other measurements of the same lava flow. The specific sample was seemingly suffered from maghemitization, possibly due to weathering. This indicates that level of oxidation or weathering varies within a lava flow, ascertaining the importance of using multiple samples in the palaeointensity experiments.

4 DISCUSSION

4.1 Alteration during KTT experiments

The surface of Tmt grains exhibited a bluish false colour at $\sim 300^\circ\text{C}$ during the KTT experiment, which was caused by a rugged, multi-stripped surface (Figs 3c, d and h). We were unable to identify the chemical component of the striped structure by elemental analysis or mapping using EDS, due to its too fine scale. Nevertheless, formation of the striped structure demonstrated that surface oxidation of Tmt occurred at temperatures as low as 300°C . If the oxidation involved iron removal, similar to the natural maghemitization of submarine basalt, then the stripes would form from the migrated iron, which would be converted to Hem. On the other hand, based on gravimetric monitoring by O'Donovan & O'Reilly (1977), O'Reilly (1983) suggested that low-temperature oxidation occurs through the addition of oxygen to Tmt during laboratory heating in air. We think that the latter process occurred in this study. In that case, irregular striped forms would also appear because the chemically bounded oxygen would form an extension of the crystal lattice on the grain surface. The mottled pattern with many microfractures in the sub-surface layer (Figs 3j and l) was probably related to the oxidation process.

A similar oxidation process with a much larger rate must have continued up to 560°C in the case of MY070132 (Figs 2 and 4). Although the subsurfaces of the severely altered Tmt grains appeared normal under optical microscopy (last photographs of Figs 2a–c) and low- to medium-magnification SEM (Figs 4c, g, h and k), high-magnification SEM revealed a mottled appearance with many whisker-like microfractures (Figs 4d and l). These microfractures indicated that the oxidation process involved not only the top surface, but also deeper subsurface layers. The results in Figs 1–4 indicated that Tmt was highly sensitive to surface oxidation. This fact was demonstrated by Lattard *et al.* (2012), although they used higher heating temperatures ($500\text{--}700^\circ\text{C}$) and observed high- rather than low-temperature oxidation.

Maghemitized parts of Tmt showed a different appearance during the KTT experiment below 400°C , with the typical grey-to-bluish colour of the Tmh parts becoming brownish at $\sim 300^\circ\text{C}$. This colour change was thought to be due to inversion of Tmh. This interpretation was supported by $\chi - T$ and $M_S - T$ curves obtained from sister samples (Fig. 9). All of the results in Fig. 9(a) showed the typical indications of inversion of Tmh at $300\text{--}400^\circ\text{C}$. The $\chi - T$ curve in air with increasing temperatures (second graph from the left) most clearly indicated that inversion of Tmh started at $200\text{--}300^\circ\text{C}$. The increase of M_S during the progressive heating in helium (rightmost graph) started at a higher temperature ($300\text{--}400^\circ\text{C}$), probably due to differences in the samples.

The inversion product was a mixture of Tmt with lower Usp content and Ilm, if the oxidation state of the originally Tmh part was assumed to be zone 1 of O'Reilly (1983), which is a low-oxidation state of maghemitization. After inversion, the surface of the originally Tmh part was very smooth when viewed by high magnification (Fig. 3g). This smooth surface indicated that the structures of the mixture of Tmt and Ilm were too fine to be detected, as was the case of the inversion of artificial Tmh powder investigated by Özdemir (1987). Strangely, the high-magnification BSE image of the sub-surface of the originally Tmh part (Fig. 3l) was almost the same as that of the originally Tmt host with many microfractures (Fig. 3j). One interpretation of this finding may be that further oxidation proceeded in the inversion product (Tmt with lower Usp content), and the oxidation process was essentially the same as that which occurred in the original Tmt host. As mentioned earlier, the microfractures in the originally Tmt and Tmh parts were presumed to be the products of alteration during the KTT experiments because the Tmt and Tmh parts of the pristine sister samples lacked this feature (Figs 3m–p).

It could be argued that all of the observations in this study are only applicable to the Tmt grains distributed on the surface or in the thin surface part of the samples, and are not directly related to the results of the Arai plots. However, there seemed to be a distinct correlation between the change of surface appearance of Tmt grains and the initiation of scatter in the Arai plot (Figs 1c and 2d). The change in surface appearance also seemed to coincide with the change in the χ -step curves. Because inversion of Tmh at $\sim 300^\circ\text{C}$ should occur throughout the whole sample, the correlation between the microscope observation and the Arai plot of CP0106B is to be expected (Fig. 1).

In the case of Tmh-free MY070132 the increase in TRM capacity and decrease in χ started at $\sim 400^\circ\text{C}$ (Fig. 2d), coincident with the start of the severe change of surface appearance of Tmt grains. The $\chi - T$ and $M_S - T$ curves of sister samples of MY070132 (Fig. 9b) were not as conspicuous as those of CP01 (Fig. 9a). The curves to increasingly elevated temperatures began to change at $400\text{--}500^\circ\text{C}$ for χ in air (second graph from the left) and $300\text{--}400^\circ\text{C}$ for M_S in vacuum (rightmost graph). All these results indicated that the microscopically observed alteration of Tmt grains on the surface was similarly occurring inside the sample during laboratory heating.

Arai plot analyses are detailed in Table 2. The palaeointensity of $8.4\ \mu\text{T}$ obtained from CP0106B is obviously unacceptable due to the prevalent occurrence of Tmh within the sample. Using typical acceptance criteria (e.g. Kissel & Laj 2004), we rejected the result because of the large MAD (mean angular deviation), large α (angular difference from the origin on the orthogonal plot) of the selected NRM component and small f (fraction of NRM for

Table 2. Results of KTT experiments.

Sample	$T_1\text{--}T_2$ ($^\circ\text{C}$)	n	$-r$	$-b$	σ_b/b	MAD ($^\circ$)	α ($^\circ$)	f	CDRAT	q	F_L (μT)	F (μT)
CP0106B	75–200	6	0.981	0.419	0.10	10.9	16.9	0.24	–0.05	1.5	20	8.4^a
MY070132	150–400	6	0.999	1.493	0.02	3.8	5.9	0.29	0.15	11.3	50	74.6^b

Note: T_1 , T_2 , lower and upper temperatures for the linear segment; n , number of data points included in the linear regression; r , correlation coefficient of the linear segment; b , slope of the segment; σ_b , standard error of b ; MAD, mean angular deviation of the selected NRM component; α , difference angle of the selected NRM component from the origin on the orthogonal plot; f , fraction of NRM for the linear segment; CDRAT, cumulative difference ratio; q , quality factor; F_L , laboratory field strength; F , palaeointensity.

^aPrevious result for this lava flow (CP01) is $10 \pm 2\ \mu\text{T}$ ($N = 2$) by Tanaka & Kono (2002), which should be regarded as unreliable due to prevalent occurrence of maghemitization.

^bExpected value for the site locality (34.1°N , 139.5°E) of this 1983 lava flow (MY07) is $45\ \mu\text{T}$ according to DGRF1985.

the linear segment). Nevertheless, the palaeointensity was consistent with the result of $10 \pm 2 \mu\text{T}$ obtained from two specimens by Tanaka & Kono (2002), in which all of acceptance criteria were cleared. Hence, this is a cautionary case that the linear data points below the critical temperature at which the alteration starts are not necessarily reliable if the sample contains Tmh. This is because, in that case, it signifies that the sample may not hold a pure TRM and hence should not have been used in the palaeointensity study. Thus, we recommend that the sample be microscopically observed when severe changes in the TRM capacity or χ -step curve occur at 300–400 °C.

We obtained a very high palaeointensity for MY070132 ($74.6 \mu\text{T}$), 66 per cent higher compared to the expected value ($45 \mu\text{T}$) at the site locality according to DGRF85 (IAGA WG V 2010). This result was rejected due to a small f and large values of DRAT and CDRAT (cumulative DRAT covering the linear segment). Nevertheless, this is another cautionary case in which the KTT experiment sometimes gives an intensity value that is too high, a problem that has been one of the most controversial theme in the community (e.g. Valet 2003).

First interpretation of the high palaeointensity and the concave-up appearance of the Arai plot (Fig. 2d) is the MD effect as the cause. Concave-up Arai plot as a manifestation of MD-like behaviour has been a major issue in the community and is no longer viable to be dismissed (e.g. Shcherbakov & Shcherbakova 2001; Calvo *et al.* 2002; Biggin & Thomas 2003; Coe *et al.* 2004; Chauvin *et al.* 2005; Biggin *et al.* 2007; Michalk *et al.* 2010). It is well known that, in the concave-up Arai plot from MD remanence, the slope between the initial point (full NRM) and the endpoint (full TRM) gives a correct palaeointensity (e.g. fig. 9.8 of Dunlop & Özdemir 1997). In the case of MY070132 the endpoint comes at 1.3 on the abscissa, and this is quite close to 1.1, the ratio of the laboratory field ($50 \mu\text{T}$) to the expected field ($45 \mu\text{T}$). This gives $38 \mu\text{T}$, which is only 15 per cent lower than the expected value and the difference would be explained by alteration occurred over 400 °C as evidenced by the displaced point at 480 °C pTRM test.

Nevertheless, we prefer an alternative interpretation that the concave-up appearance of the Arai plot was largely due to deflected data points over 400 °C that were caused by the alteration. This is based on the results of the microscopic observation, moderate change in χ -step curve, and the PSD nature on the Day plot (Appendix). A concave-up Arai plot may not necessarily be due to the MD effect (e.g. Paterson 2011; Tanaka *et al.* 2012). High slope under low temperatures often gives a concave-up appearance, which seems to be the case for MY070132. Causes of the low temperature high slope may include decay of viscous remanence (Coe 1967b), physical change of the domain state in PSD grains (Kosterov & Prévot 1998) and thermochemical remanent magnetization (TCRM) as an intrinsic NRM origin (Yamamoto *et al.* 2003; Yamamoto 2006; Yamamoto & Hoshi 2008). Given that MY070132 contains highly oxidized Tmt grains (Fig. 2c), similar to the Hawaiian 1960 lava studied by Yamamoto *et al.* (2003), it is possible that natural TCRM caused the high palaeointensity. Nevertheless, we cannot exclude the possibility that the Tmt grains began to be altered at low temperatures of 250–300 °C, as evidenced by the false blue colour (Figs 2a and b), and that this process somehow diminished the magnitude of NRM.

4.2 Alteration at 610 °C

In a second series of experiments, we heated the samples in air at 610 °C for increasing times. After the 50-min run, a mottled pattern

appeared in the Tmt part of OT572261 under optical microscopy. After 200 min run, the mottled pattern became more discernible (Fig. 5). We could not identify the dark patch in the BSE image due to its too-fine scale (Figs 6b, e and f). It could be that Ilm precipitated during high-temperature oxidation, based on its darker shade than the Tmt part. However, after its initial increase by 20 per cent, χ remained constant throughout the experiments, which may have precluded the creation of Tmt close to Mt by high-temperature oxidation. This possibility is supported by the completely reproducible $\chi - T$ and $M_s - T$ curves (Fig. 9c except for the second graph from the left-hand side, in which the sample was seemingly suffered from maghemitization). Gehring *et al.* (2009) reported a similar mottled pattern in Tmt grains contained in basalt-originated dune sand. They identified Si along with Al and Ca in the mottled patch, which was interpreted as migration from silicate into Ti-poor parts during high-temperature oxidation. In any case, the result suggested that the rate of oxidation of Tmt grain when heated at 610 °C in air was on the order of tens of minutes. This timing confirms the importance of minimizing the heating time in the palaeointensity experiment, which is the basis for variations of the KTT method with single heating steps (Kono & Ueno 1977), a multispecimen method (Hoffman *et al.* 1989) and a microwave method (Walton *et al.* 1993).

It took only 10 min for the trellis-type structure to appear in the case of the completely maghemitized Tmt grain of OT580411 (Fig. 7). It is important to note that the trellis-type structure was not a product of the high-temperature oxidation of Tmt, but of Tmh inversion, as indicated by the curves of $\chi - T$ and $M_s - T$ (Fig. 9d). This near-instantaneous occurrence of Tmh inversion is reasonable in light of its small activation energy of 0.033 eV, measured from thermomagnetic analysis using a submarine basalt, by Ozima & Ozima (1972). The low activation energy for unmixing of Tmh is contrasted to that of 2.2 eV for interdiffusion of Fe and Ti cations, applicable to high-temperature oxidation of Tmt, by Freer & Hauptman (1978).

We could not identify the chemical components of the inversion product due to its too-fine structure (Fig. 8d), but we think that the trellis part was Hem rather than Ilm. The trellis had a lighter shade in the BSE image than the original thick and fine Ilm lamellae, indicating elements with higher mean atomic number compared to Ilm. The host part must be Mt, although its shade was darker than the trellis in spite of the larger mean atomic number of Mt compared to Hem. The darker shade was probably caused by the uneven surface of the grain. Inversion products of similar Hem lamellae were observed by Ozima & Larson (1967) in partially maghemitized Tmt gains of subaerial andesite rock when the sample was heated under vacuum. Inversion of Tmh accompanied by production of Hem indicates that the oxidation level of Tmh was fairly high of zone 3, according to O'Reilly (1983).

As discussed in the previous section, the presence of Tmh is hazardous in KTT experiments because the inversion temperature could be misinterpreted as the critical temperature under which the data points can be included in the analysis, although in reality the sample may not hold a pure TRM and hence should not have been used in the experiments. The presence of Tmh is also problematic in Shaw experiments. Even if the inversion of Tmh occurs when laboratory TRM is induced, the ARM-corrected Shaw plot could appear reasonably linear, due to the proportionality between the changes of TRM and ARM and the general insensitivity of the alternating field spectra to the change of blocking temperature (Tanaka & Komuro 2009). In the case of the sister sample OT58-4-5 (fig. 5 of Tanaka & Komuro 2009), the ARM-corrected Shaw plot was fairly linear,

although it was successfully rejected by the criteria of Yamamoto *et al.* (2003).

4.3 Alteration as a low-temperature oxidation process

We demonstrated the alteration of Tmt grain during KTT experiments and laboratory heating at 610 °C in air. A considerable change in morphology was observed in the polished surface and near subsurface. The surface oxidation was clearly not in equilibrium, as is the case for the high-temperature oxidation at 1300 °C (Lattard *et al.* 2012). It has often been suggested that in the laboratory heating of volcanic rocks, trellis-type Ilm lamellae are newly created in Tmt grains due to high-temperature oxidation, leading to a change of TRM capacity. However, actual microscopic observation has been rarely reported. We also failed to observe this event in this study. Other studies may have attributed the formation of Ilm lamellae to higher heating temperature (Strangway *et al.* 1968) or longer heating time (Davis & Evans 1976) or both (Saito 2005). Holm & Verosub (1988) reported the creation of Ilm lamellae in Tmt grains contained in marine sediments at temperatures as low as 200 °C, although this occurrence was probably an exceptional case that occurred in a specific sediment in which magnetic grains were extremely susceptible to high-temperature oxidation. In any case, it seems that typical high-temperature oxidation forming trellis-type Ilm lamellae is not easily attained in solid volcanic rocks during short laboratory heating at temperatures at or below ~600 °C.

It is generally believed that low-temperature oxidation does not proceed in laboratory heating in air unless the material is very fine Tmt grains ballmilled in water (Nishitani & Kono 1982). In fact, the magnetic properties of Tmh reported by Akimoto *et al.* (1957) were later denied because the heating of sintered Tmt material in air at 400–500 °C would produce products of high-temperature oxidation (Ozima & Larson 1970). Nevertheless, based on the observations in this study, we think that the oxidation process on the Tmt surface during laboratory heating below ~400 °C is closer to a low- than to a high-temperature oxidation. In fact, Creer *et al.* (1970) suspected that low-temperature oxidation occurred when basalt samples were heated at 400 °C in air.

It is usually considered that water is necessary for low-temperature oxidation to proceed. However, the presence of Tmh has sometimes been reported in situations where no water circulation was expected. Non-stoichiometric Tmt (i.e. Tmh) has been reported to form at temperatures of 1275 °C during laboratory syntheses (Hauptman 1974) or below 500 °C during the primary cooling of the Olby Basalt, France (Krása *et al.* 2005). Gehring *et al.* (2009) found aggregates of Mt and maghemite (Mh) in the host part of high-temperature oxidized Tmt in basalt-originated dune sand, suggesting that Mh formed from Mt by oxidative alteration under an arid climate. Formation of Tmh was reported in Icelandic lavas, which suffered heating from dyke intrusion (Kristjánsson 1985; Gunnlaugsson *et al.* 2008). The last case of dyke intrusion is probably closest to the oxidation process of Tmt during the KTT experiment in air under ~400 °C, as observed in this study.

5 CONCLUSIONS

Tmt grains on the polished surface of volcanic rocks were microscopically observed during KTT experiments in air. Changes in the colour and morphology of the Tmt surface were observed at

a fairly low step temperature of 300 °C, and they became more pronounced as the experiment proceeded. Although observations were made from the top surfaces of the samples, similar oxidation of Tmt must have occurred inside the samples because grain surface changes were notably correlated with the scatter of data points on the Arai plot. In a second experiment, samples were heated at 610 °C in air for increasing times from 10 to 500 min. We observed the gradual alteration of Tmt by microscopy. Many patches and whisker-like microfractures of submicron size were created during heating, but the creation of new Ilm lamellae was not observed, even after a 500 min heating run. Taken together, these results allow us to conclude that typical high-temperature oxidation forming trellis-type Ilm lamellae is not easily attained during laboratory heating in air at temperatures at or below ~600 °C, and that alteration under ~400 °C is closer to a low- than to a high-temperature oxidation process. On the other hand, inversion of the maghemitized part of Tmt occurs instantaneously at 300 °C during the KTT experiment, and when heated in the laboratory at 610 °C, the trellis-type structure emerges only after 10 min. Inversion of the maghemitized part of Tmt is hazardous in the KTT experiment because the inversion temperature can be misinterpreted as the critical temperature under which the data points can be included in the palaeointensity analysis, even though the sample may not hold a pure TRM and should not have been used.

ACKNOWLEDGEMENTS

We thank Hideo Nakanishi for use of the optical microscope and Takuya Matsuzaki for instruction in SEM. We appreciate the many instructive comments provided by two reviewers, Mark Dekkers and Greig Paterson, and the editor, Andrew Biggin, which much improved the original manuscript. This study was financially supported by the Kochi University Research Project 'Research Center for Global Environmental Change by Earth Drilling Sciences'.

REFERENCES

- Akimoto, S. & Kushiro, I., 1960. Natural occurrence of titanomaghemite and its relevance to the unstable magnetization of rocks, *J. Geomagn. Geoelectr.*, **11**, 94–110.
- Akimoto, S., Katsura, T. & Yoshida, M., 1957. Magnetic properties of $\text{TiFe}_2\text{O}_4\text{-Fe}_3\text{O}_4$ system and their change with oxidation, *J. Geomagn. Geoelectr.*, **9**, 165–178.
- Allan, J.E.M., Coey, J.M.D., Sanders, I.S., Schwertmann, U., Friedrich, G. & Wiechowski, A., 1989. An occurrence of a fully-oxidized natural titanomaghemite in basalt, *Mineral. Mag.*, **53**, 299–304.
- Biggin, A.J. & Thomas, D.N., 2003. The application of acceptance criteria to results of Thellier palaeointensity experiments performed on samples with pseudo-single-domain-like characteristics, *Phys. Earth planet. Inter.*, **138**, 279–287.
- Biggin, A.J., Perrin, M. & Dekkers, M.J., 2007. A reliable absolute palaeointensity determination obtained from a non-ideal recorder, *Earth planet. Sci. Lett.*, **257**, 545–563.
- Buddington, A.F. & Lindsley, D.H., 1964. Iron-titanium oxide minerals and synthetic equivalents, *J. Petrol.*, **5**, 310–357.
- Calvo, M., Prévot, M., Perrin, M. & Riisager, J., 2002. Investigating the reasons for the failure of palaeointensity experiments: a study on historical lava flows from Mt. Etna (Italy), *Geophys. J. Int.*, **149**, 44–63.
- Chauvin, A., Roperch, P. & Levi, S., 2005. Reliability of geomagnetic paleointensity data: the effects of the NRM fraction and concave-up behavior on paleointensity determinations by the Thellier method, *Phys. Earth planet. Inter.*, **150**, 265–286.

- Chen, T., Xu, H., Xie, Q., Chen, J., Ji, J. & Lu, H., 2005. Characteristics and genesis of maghemite in Chinese loess and paleosols: mechanism for magnetic susceptibility enhancement in paleosols, *Earth planet. Sci. Lett.*, **240**, 790–802.
- Coe, R.S., 1967a. Paleo-intensity of the earth's magnetic field determined from Tertiary and Quaternary rocks, *J. geophys. Res.*, **72**, 3247–3262.
- Coe, R.S., 1967b. The determination of paleo-intensities of the earth's magnetic field with emphasis on mechanisms which could cause non-ideal behavior in Thellier's method, *J. Geomagn. Geoelectr.*, **19**, 157–179.
- Coe, R.S., Riisager, J., Plenier, G., Leonhardt, R. & Krása, D., 2004. Multidomain behavior during Thellier paleointensity experiments: results from the 1915 Mt. Lassen flow, *Phys. Earth planet. Inter.*, **147**, 141–153.
- Creer, K.M. & Petersen, N., 1969. Thermochemical magnetisation in basalts, *Z. Geophys.*, **35**, 501–516.
- Creer, K.M., Petersen, N. & Petherbridge, J., 1970. Partial self-reversal of remanent magnetization and anisotropy of viscous magnetization in Basalts, *Geophys. J. R. astr. Soc.*, **21**, 471–483.
- Davis, P.M. & Evans, M.E., 1976. Interacting single-domain properties of magnetite intergrowths, *J. geophys. Res.*, **81**, 989–994.
- Day, R., Fuller, M. & Schmidt, V.A., 1977. Hysteresis properties of titanomagnetites: grain-size and compositional dependence, *Phys. Earth planet. Inter.*, **13**, 260–267.
- Dunlop, D.J., 2002. Theory and application of the Day plot (M_{rs}/M_s versus H_{cr}/H_c) 1. Theoretical curves and tests using titanomagnetite data, *J. geophys. Res.*, **107**, doi: 10.1029/2001JB000486.
- Dunlop, D.J., 2012. Magnetic recording in rocks, *Phys. Today*, **65**, 31–37.
- Dunlop, D.J. & Özdemir, Ö., 1997. *Rock Magnetism: Fundamentals and Frontiers*, Cambridge Univ. Press.
- Freer, R. & Hauptman, Z., 1978. An experimental study of magnetite-titanomagnetite interdiffusion, *Earth planet. Sci. Lett.*, **16**, 223–231.
- Furuta, T., Otsuki, M. & Akimoto, T., 1985. Quantitative electron probe microanalysis of oxygen in titanomagnetites with implications for oxidation processes, *J. geophys. Res.*, **90**, 3145–3150.
- Gehring, A.U., Fischer, H., Louvel, M., Kunze, K. & Weidler, P.G., 2009. High temperature stability of natural maghemite: a magnetic and spectroscopic study, *Geophys. J. Int.*, **179**, 1361–1371.
- Gunnlaugsson, H.P., Rasmussen, H., Kristjánsson, L., Steinthorsson, S., Helgason, Ö., Nornberg, P., Madsen, M.B. & Mørup, S., 2008. Mössbauer spectroscopy of magnetic minerals in basalt on Earth and Mars, *Hyp. Int.*, **182**, 87–101.
- Haggerty, S.E., 1991. Oxide textures: a mini-atlas, in *Reviews in Mineralogy Volume 25—Oxide Minerals: Petrologic and Magnetic Significance*, pp. 129–219, ed. Lindsley, D.H., Mineralogical Society of America.
- Hauptman, Z., 1974. High temperature oxidation, range of non-stoichiometry and Curie point variation of cation deficient titanomagnetite $\text{Fe}_{2.4}\text{Ti}_{0.6}\text{O}_{4+\gamma}$, *Geophys. J. R. astr. Soc.*, **38**, 29–47.
- Hoffman, K.A., Constantine, V.L. & Morse, D.L., 1989. Determination of absolute palaeointensity using a multi-specimen procedure, *Nature*, **339**, 295–297.
- Holm, E.J. & Verosub, K.L., 1988. An analysis of the effects of thermal demagnetization on magnetic carriers, *Geophys. Res. Lett.*, **15**, 487–490.
- IAGA Working Group V-MOD, 2010. International Geomagnetic Reference Field: the eleventh generation, *Geophys. J. Int.*, **183**, 1216–1230.
- Johnson, H.P. & Atwater, T., 1977. Magnetic study of basalts from the Mid-Atlantic Ridge, lat. 37°N, *Geol. Soc. Am. Bull.*, **88**, 637–647.
- Kent, D.V. & Lowrie, W., 1974. Origin of magnetic instability in sediment cores from the central North Pacific, *J. geophys. Res.*, **79**, 2987–3000.
- Kissel, C. & Laj, C., 2004. Improvements in procedure and paleointensity selection criteria (PICRIT-03) for Thellier and Thellier determinations: application to Hawaiian basaltic long cores, *Phys. Earth planet. Inter.*, **147**, 155–169.
- Königsberger, J.G., 1938. Natural residual magnetism of eruptive rocks, *Terr. Magn. Atmos. Elect.*, **43**, 199–127, 299–320.
- Kono, M., 1978. Reliability of palaeointensity methods using alternating field demagnetization and anhysteretic remanence, *Geophys. J. R. astr. Soc.*, **54**, 241–261.
- Kono, M., 1985. Changes in magnetic hysteresis properties of a basalt induced by heating in air, *J. Geomagn. Geoelectr.*, **37**, 589–600.
- Kono, M., 1987. Changes in TRM and ARM in a basalt due to laboratory heating, *Phys. Earth planet. Inter.*, **46**, 1–8.
- Kono, M. & Tanaka, H., 1977. Influence of partial pressure of oxygen on thermoremanent magnetization of basalts, *Phys. Earth planet. Inter.*, **13**, 276–288.
- Kono, M. & Ueno, N., 1977. Paleointensity determination by a modified Thellier method, *Phys. Earth planet. Inter.*, **13**, 305–314.
- Kosterov, A.A. & Prévot, M., 1998. Possible mechanisms causing failure of Thellier palaeointensity experiments in some basalts, *Geophys. J. Int.*, **134**, 554–572.
- Krásá, D., Shcherbakov, V.P., Kunzmann, T. & Petersen, N., 2005. Self-reversal of remanent magnetization in basalts due to partially oxidized titanomagnetites, *Geophys. J. Int.*, **162**, 115–136.
- Kristjánsson, L., 1985. Magnetic and thermal effects of dike intrusions in Iceland, *J. geophys. Res.*, **90**, 10 129–10 135.
- Larson, E., Ozima, M., Ozima, M., Nagata, T. & Strangway, D., 1969. Stability of remanent magnetization of igneous rocks, *Geophys. J. R. astr. Soc.*, **17**, 263–292.
- Lattard, D., Sauerzapf, U. & Kontny, A., 2012. Rapid surficial oxidation of synthetic Fe-Ti oxides at high temperature: observations and consequences for magnetic measurements, *Geochem. Geophys. Geosyst.*, **13**, doi:Q08Z46/2012GC004152.
- Liu, X.M., Shaw, J., Liu, T.S., Heller, F. & Yuan, B.Y., 1992. Magnetic mineralogy of Chinese loess and its significance, *Geophys. J. Int.*, **108**, 301–308.
- Marshall, M. & Cox, A., 1972. Magnetic changes in pillow basalt due to sea floor weathering, *J. geophys. Res.*, **77**, 6459–6469.
- Michalk, D.M., Biggin, A.J., Knudsen, M.F., Bohnel, H.N., Nowaczyk, N.R., Ownby, S. & Lopez-Martinez, M., 2010. Application of the multi-specimen palaeointensity method to Pleistocene lava flows from the Trans-Mexican Volcanic Belt, *Phys. Earth planet. Inter.*, **179**, 139–156.
- Nagata, T., Arai, Y. & Momose, K., 1963. Secular variation of the geomagnetic total force during the last 5000 years, *J. geophys. Res.*, **68**, 5277–5281.
- Nishitani, T. & Kono, M., 1982. Grain size effect on the low-temperature oxidation of titanomagnetite, *J. Geophys.*, **50**, 137–142.
- O'Donovan, J.B. & O'Reilly, W., 1977. Range of non-stoichiometry and characteristic properties of the products of laboratory maghemitization, *Earth planet. Sci. Lett.*, **34**, 291–299.
- O'Reilly, W., 1983. The identification of titanomaghemites: model mechanisms for the maghemitization and inversion processes and their magnetic consequences, *Phys. Earth planet. Inter.*, **31**, 65–76.
- Özdemir, Ö., 1987. Inversion of titanomaghemites, *Phys. Earth planet. Inter.*, **46**, 184–196.
- Ozima, M., 1971. Magnetic processes in oceanic ridge, *Earth planet. Sci. Lett.*, **13**, 1–5.
- Ozima, M. & Larson, E.E., 1967. Study on irreversible change of magnetic properties of some ferromagnetic minerals, *J. Geomagn. Geoelectr.*, **19**, 117–127.
- Ozima, M. & Larson, E.E., 1970. Low-and high-temperature oxidation of titanomagnetite in relation to irreversible changes in the magnetic properties of submarine basalts, *J. geophys. Res.*, **75**, 1003–1017.
- Ozima, M. & Ozima, M., 1972. Activation energy of unmixing of titanomagnetite, *Phys. Earth planet. Inter.*, **5**, 87–89.
- Paterson, G.A., 2011. A simple test for the presence of multidomain behavior during paleointensity experiments, *J. geophys. Res.*, **116**, doi:10.1029/2011JB008369.
- Petersen, N. & Hojatollah, V., 1987. Observation of shrinkage cracks in ocean floor titanomagnetites, *Phys. Earth planet. Inter.*, **46**, 197–205.
- Rolph, T.C. & Shaw, J., 1985. A new method of paleofield magnitude correction for thermally altered samples and its application to Lower Carboniferous lavas, *Geophys. J. R. astr. Soc.*, **80**, 773–781.
- Ryall, P.J.C. & Hall, J.M., 1980. Iron loss in titanomagnetites during low temperature oxidation, *J. Geomagn. Geoelectr.*, **32**, 661–669.
- Saito, T., 2005. Magnetic petrology: application to volcanology, *J. Geography*, **114**, 296–308. (In Japanese)

- Shaw, J., 1974. A new method of determining the magnitude of the palaeomagnetic field, application to five historic lavas and five archaeological samples, *Geophys. J. R. astr. Soc.*, **39**, 133–141.
- Shcherbakov, V.P. & Shcherbakova, V.V., 2001. On the suitability of the Thellier method of palaeointensity determinations on pseudo-single-domain and multidomain grains, *Geophys. J. Int.*, **146**, 20–30.
- Strangway, D.W., Larson, E.E. & Goldstein, M., 1968. A possible cause of high magnetic stability in volcanic rocks, *J. geophys. Res.*, **73**, 3787–3795.
- Tanaka, H. & Kono, M., 2002. Paleointensities from a Cretaceous basalt platform in Inner Mongolia, northeastern China, *Phys. Earth planet. Inter.*, **133**, 147–157.
- Tanaka, H. & Komuro, N., 2009. The Shaw paleointensity method: can the ARM simulate the TRM alteration? *Phys. Earth planet. Inter.*, **173**, 269–278.
- Tanaka, H., Hashimoto, Y. & Morita, N., 2012. Palaeointensity determinations from historical and Holocene basalt lavas in Iceland, *Geophys. J. Int.*, **189**, 833–845.
- Tauxe, L. & Yamazaki, T., 2007. Paleointensities, in *Treatise on Geophysics*, Vol. 5, pp. 509–563, ed. Kono, M., Geomagnetism, Elsevier.
- Thellier, E. & Thellier, O., 1959. Sur l'intensité du champ magnétique terrestre dans le passé historique et géologique, *Ann. Geophys.*, **15**, 285–376.
- Valet, J.-P., 2003. Time variations in geomagnetic intensity, *Rev. Geophys.*, **41**, doi:10.1029/2001RG000104.
- Walton, D., Share, J., Rolph, T.C. & Shaw, J., 1993. Microwave magnetisation, *Geophys. Res. Lett.*, **20**, 109–111.
- Watkins, N.D. & Haggerty, S.E., 1967. Primary oxidation variation and petrogenesis in a single lava, *Contr. Mineral. Petrol.*, **15**, 251–271.
- Wilson, R.L. & Watkins, N.D., 1967. Correlation of petrology and natural magnetic polarity in Columbia Plateau basalts, *Geophys. J. R. astr. Soc.*, **12**, 405–424.
- Yamamoto, Y., 2006. Possible TCRM acquisition of the Kilauea 1960 lava, Hawaii: failure of the Thellier paleointensity determination inferred from equilibrium temperature of the Fe-Ti oxide, *Earth Planets Space*, **58**, 1033–1044.
- Yamamoto, Y. & Hoshi, H., 2008. Paleomagnetic and rock magnetic studies of the Sakurajima 1914 and 1946 andesitic lavas from Japan: a comparison

of the LTD-DHT Shaw and Thellier paleointensity methods, *Phys. Earth planet. Inter.*, **167**, 118–143.

Yamamoto, Y., Tsunakawa, H. & Shibuya, H., 2003. Paleointensity study of the Hawaiian 1960 lava: implications for possible causes of erroneously high intensities, *Geophys. J. Int.*, **153**, 263–276.

APPENDIX: DAY PLOT OF HYSTERESIS PARAMETERS

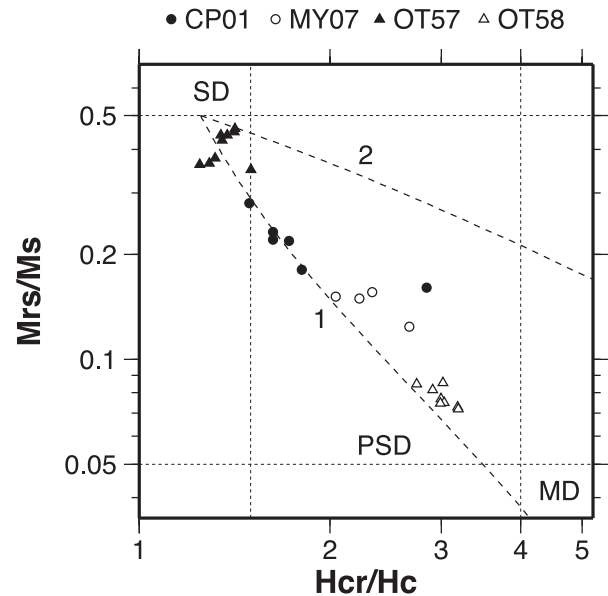


Figure A1. Day plot of magnetic hysteresis parameters measured in the sister samples of the four samples used in this study. Both abscissa and ordinate are in log scaling. The dashed curves, 1 and 2, are mixing curves of SD–MD and SD–SP (10 nm) from Dunlop (2002), respectively.